Identification and Decoupling Control of Flexure Jointed Hexapods

Yixin Chen & John E. McInroy

University of Wyoming, Dept. of Electrical Engineering, Laramie, WY, 82071

Abstract

By exploiting properties of the joint space mass-inertia matrix of flexure jointed hexapods, a new decoupling method is proposed. The new decoupling method, through a static input-output mapping, transforms the highly coupled 6 input 6 output dynamics into 6 independent single-input single-output (SISO) channels. Controls for these SISO channels are far simpler than their multiple-input multiple-output counterparts. Prior decoupling control algorithms imposed severe constraints on the allowable geometry, workspace, and payload. This paper derives a new algorithm which removes these constraints, thus greatly expanding the applications. Based on the new decoupling algorithm, an identification algorithm is introduced to identify the joint space mass-inertia matrix using payload accelerations and base forces. This algorithm can be used for precision payload calibration, thus improving performance and removing the labor required to design the control for different payloads. The new decoupling algorithm is experimentally compared to earlier techniques. These experimental results indicate that the new approach is practical, and improves performance.

1 Introduction

Several researchers have developed flexure jointed hexapods for micro-precision applications in which only a very small workspace is required ([1], [4], [5], [10], [11], [12], [13], [14]). To avoid the extremely nonlinear micro-dynamics of joint friction and backlash, these hexapods employ flexure joints. A flexure joint bends material to achieve motion, rather than sliding or rolling across two surfaces. This does eliminate friction and backlash, but adds spring dynamics and limits the workspace. Compared to non-flexure jointed hexapods, flexure jointed hexapods have several distinct characteristics [8]: (1) The flexures greatly alter the dynamic behavior; (2) The base motion is a significant contributor to the overall motion, even when the base is subjected only to ambient seismic vibrations; (3) Because the workspace is so small, linearized dynamic models are highly accurate.

McInroy [7] developed and validated the dynamics of a flexure jointed hexapod. Using this model, [8] proposed two decoupling algorithms by combining static input-output transformations with hexapod geometric design.

These decoupling algorithms impose two constraints: (1) The payload mass-inertia matrix must be diagonal; (2) The geometry of the hexapod and the attachment of the payload to the hexapod must be carefully chosen [8]. For instance, if a mutually orthogonal geometry has been selected [9], the payload's center of mass must coincide with the center of the cube formed by the orthogonal struts ([12] provides more geometric details). Although these constraints are possible to satisfy for some specific applications, they limit the applications significantly. For instance, in order to satisfy the constraints, the payload on the University of Wyoming (UW) hexapod requires a complicated, custom designed truss structure. Any changes to the payload requires a new truss structure, so minor changes are prohibitively expensive. Moreover, the constraints limit the location of the end effector, thus eliminating some important applications such as those requiring cooperating hexapods.

The algorithm derived herein removes these constraints, thus greatly expanding the potential applications. For instance, by relaxing the geometry constraints, geometries matched to particular needs can be used. Similarly, new payloads can easily be accommodated. To further improve performance and ease of use, a Least Squares (LS) based identification algorithm is derived to estimate the joint space mass-inertia matrix from payload accelerations and base forces. This allows new payloads to be quickly incorporated without the labor and potential errors that accompany model based approaches. Furthermore, it allows precision calibration of the dynamics to increase the performance over that attained when using mod-

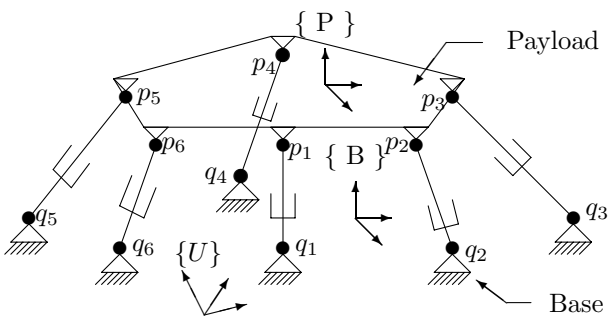

Figure 1: A flexure jointed hexapod (or Stewart Platform). $\{P\}$ is a Cartesian coordinate frame located at, and rigidly attached to, the payload's center of mass. $\{B\}$ is the frame attached to the (possibly moving) base, and $\{U\}$ is a Universal inertial frame of reference.

eled, vs. measured parameters. Experimental results on the UW hexapod indicate that the decoupling and identification algorithms are practical, and yield superior performance.

2 Dynamic Model of Flexure Jointed Hexapods

This section briefly summarizes the dynamic model of flexure jointed hexapods [7]. Figure 1 illustrates a general flexure jointed hexapod. Like any hexapod, it consists of a base, a payload, and six struts that can change their lengths. The struts, which have spherical joints at both ends, connect the payload to the base.

In the joint space, the dynamics of a flexure jointed hexapod are written as[7]

$$\vec{f_b} = \vec{f_m} - \mathbf{K}(\vec{l} - \vec{l_r}) - \mathbf{B}\dot{\vec{l}} \tag{1}$$

$$\begin{aligned}({}^U_P\mathbf{R}\,{}^P\mathbf{M}_x\,{}^B_P\mathbf{R}^T\mathbf{J}^{-1} + {}^U_B\mathbf{R}\mathbf{J}^T\mathbf{M}_s)\ddot{\vec{l}} + {}^U_B\mathbf{R}\mathbf{J}^T\mathbf{B}\dot{\vec{l}} + \\ {}^U_B\mathbf{R}\mathbf{J}^T\mathbf{K}(\vec{l} - \vec{l_r}) = {}^U_B\mathbf{R}\mathbf{J}^T\vec{f}_m + \vec{\mathcal{F}}_e + \vec{\mathcal{G}} + \vec{\mathcal{C}} - \\ ({}^U_B\mathbf{R}\mathbf{J}^T\mathbf{M}_s + {}^U_P\mathbf{R}\,{}^P\mathbf{M}_x\,{}^U_P\mathbf{R}^T\mathbf{J}_c\mathbf{J}_B{}^{-1})\ddot{\vec{q}}_s\end{aligned} \tag{2}$$

where

- $\mathbf{J}$ is the 6×6 hexapod Jacobian relating payload Cartesian movements, expressed in the $\{P\}$ frame, to strut length changes in the joint space;
- ${}^B_U\mathbf{R}$ is the 6×6 rotation matrix from the base frame, $\{B\}$, to the Universal inertial frame of reference, $\{U\}$ (it consists of two identical 3×3 rotation matrices forming a block diagonal 6×6 matrix);
- $\mathbf{J}_c$ and $\mathbf{J}_B$ are 6×6 Jacobian matrices capturing base motion;
- ${}^P\mathbf{M}_x$ is the 6×6 mass-inertia matrix of the payload found with respect to the payload frame ($\{P\}$);
- $\mathbf{M}_s$ is a diagonal 6×6 matrix containing the moving mass of each strut;
- $\mathbf{B}$ and $\mathbf{K}$ are 6×6 diagonal matrices containing the damping and stiffness, respectively, of each strut;
- $\vec{l}$ is the 6×1 vector of strut lengths, and $\vec{l_r}$ is the constant vector of relaxed strut lengths;
- $\vec{f_b}$ is the vector of forces exerted at the bottom of the strut;
- $\vec{f_m}$ is the vector of strut motor forces;
- $\ddot{\vec{q}}_s$ is a 6×1 vector of base accelerations along each strut plus some Coriolis terms;
- $\vec{\mathcal{F}}_e$ is a vector of payload exogenous generalized forces;
- $\vec{\mathcal{C}}$ is a vector containing all the Coriolis and centripetal terms except the Coriolis terms in $\ddot{\vec{q}}_s$;
- $\vec{\mathcal{G}}$ is a vector containing all gravity terms.

Since the struts can only move very small distances, the Jacobian ($\mathbf{J}$) and the rotation matrix (${}^B_P\mathbf{R}$) can be considered constant, and Coriolis terms are often negligible. The algorithms developed in this paper assume that $\mathbf{J}$ and ${}^B_P\mathbf{R}$ are constant. This does, of course, limit the applications somewhat, but is in practice highly accurate because the flexure joints severely limit the workspace anyway.

Note that the base motions play a role in the dynamic model (2) both explicitly ($\ddot{\vec{q}}_s$, ${}^U_P\mathbf{R}$, and ${}^U_B\mathbf{R}$) and implicitly (through $\ddot{\vec{l}}$, $\dot{\vec{l}}$, and $\vec{l}$). The relations among payload motion, base motion and strut dynamics can be described as [7]

$$\vec{l} = \vec{p}_s - \vec{q}_s \tag{3}$$

$$\dot{\vec{l}} = \dot{\vec{p}}_s - \dot{\vec{q}}_s \tag{4}$$

$$\ddot{\vec{l}} = \ddot{\vec{p}}_s - \ddot{\vec{q}}_s \tag{5}$$

where $\vec{p}_s = [\vec{v}_1^T\vec{p}_1, ..., \vec{v}_6^T\vec{p}_6]^T$, $\vec{q}_s = [\vec{v}_1^T\vec{q}_1, ..., \vec{v}_6^T\vec{q}_6]^T$, $\vec{p}_i$ denotes the three dimensional attachment point of the i^{th} strut to the payload and $\vec{q}_i$ denotes the attachment point of the i^{th} strut to the base (Figure 1), $\vec{v}_i$ is the unit direction vector of the i^{th} strut pointing from $\vec{q}_i$ to $\vec{p}_i$ ($\vec{p}_i$, $\vec{q}_i$, and $\vec{v}_i$ are expressed in the same coordinate frame).

Substituting (3-5) into (1-2) and rearranging terms produces the following dynamic equations

$$\vec{f}_b = \vec{f}_m - \mathbf{K}(\vec{p}_s - \vec{q}_s - \vec{l}_r) - \mathbf{B}(\dot{\vec{p}}_s - \dot{\vec{q}}_s) \qquad (6)$$

$$\begin{aligned}({}^U_P\mathbf{R}\,{}^P\mathbf{M}_x\,{}^B_P\mathbf{R}^T\mathbf{J}^{-1} + {}^U_B\mathbf{R}\mathbf{J}^T\mathbf{M}_s)\ddot{\vec{p}}_s + {}^U_B\mathbf{R}\mathbf{J}^T\mathbf{B}\dot{\vec{p}}_s + \\ {}^U_B\mathbf{R}\mathbf{J}^T\mathbf{K}\vec{p}_s = {}^U_B\mathbf{R}\mathbf{J}^T\vec{f}_m + \vec{\mathcal{F}}_e + \vec{\mathcal{G}} + \vec{\mathcal{C}} + \\ ({}^U_P\mathbf{R}\,{}^P\mathbf{M}_x\,{}^B_P\mathbf{R}^T\mathbf{J}^{-1} - {}^U_P\mathbf{R}\,{}^P\mathbf{M}_x\,{}^U_P\mathbf{R}^T\mathbf{J}_c\mathbf{J}_B{}^{-1})\ddot{\vec{q}}_s + \\ {}^U_B\mathbf{R}\mathbf{J}^T\mathbf{B}\dot{\vec{q}}_s + {}^U_B\mathbf{R}\mathbf{J}^T\mathbf{K}(\vec{q}_s + \vec{l}_r). \qquad (7)\end{aligned}$$

For the small movements possible in flexure jointed hexapods, $\mathbf{J}$, $\mathbf{J}_c$, $\mathbf{J}_B$, and ${}^B_P\mathbf{R}$ are all nearly constant. For small base motions, ${}^U_B\mathbf{R}$, ${}^U_P\mathbf{R}$, and $\vec{\mathcal{G}}$ are also constant, while $\vec{\mathcal{C}}$ can be neglected because large velocities cannot be attained in the small distance moved. The remainder of this paper will assume small base motions for brevity, but large base motions can be treated by incorporating ${}^U_B\mathbf{R}$ and feeding forward $\vec{\mathcal{G}}$ and $\vec{\mathcal{C}}$ terms.

By letting the spring compression absorb the static gravity forces, both $\vec{l}_r$ and $\vec{\mathcal{G}}$ terms can be removed. Thus (7) can be written as the following linear time invariant (LTI) equation

$$\begin{aligned}({}^U_P\mathbf{R}\,{}^P\mathbf{M}_x\,{}^B_P\mathbf{R}^T\mathbf{J}^{-1} + {}^U_B\mathbf{R}\mathbf{J}^T\mathbf{M}_s)\ddot{\vec{p}}_s + {}^U_B\mathbf{R}\mathbf{J}^T\mathbf{B}\dot{\vec{p}}_s + \\ {}^U_B\mathbf{R}\mathbf{J}^T\mathbf{K}\vec{p}_s = {}^U_B\mathbf{R}\mathbf{J}^T\vec{f}_m + \vec{\mathcal{F}}_e + \\ ({}^U_P\mathbf{R}\,{}^P\mathbf{M}_x\,{}^B_P\mathbf{R}^T\mathbf{J}^{-1} - {}^U_P\mathbf{R}\,{}^P\mathbf{M}_x\,{}^U_P\mathbf{R}^T\mathbf{J}_c\mathbf{J}_B{}^{-1})\ddot{\vec{q}}_s + \\ {}^U_B\mathbf{R}\mathbf{J}^T\mathbf{B}\dot{\vec{q}}_s + {}^U_B\mathbf{R}\mathbf{J}^T\mathbf{K}\vec{q}_s. \qquad (8)\end{aligned}$$

Multiplying both sides of (8) by $\mathbf{J}^{-T}{}^U_B\mathbf{R}^T$, it can be written as

$$\begin{aligned}\mathbf{M}_p\ddot{\vec{p}}_s + \mathbf{B}\dot{\vec{p}}_s + \mathbf{K}\vec{p}_s = \vec{f}_m + \\ \mathbf{M}_q\ddot{\vec{q}}_s + \mathbf{B}\dot{\vec{q}}_s + \mathbf{K}\vec{q}_s + \mathbf{J}^{-T}{}^U_B\mathbf{R}^T\vec{\mathcal{F}}_e \qquad (9)\end{aligned}$$

where

$$\begin{aligned}\mathbf{M}_p &= \mathbf{J}^{-T}{}^B_P\mathbf{R}\,{}^P\mathbf{M}_x\,{}^B_P\mathbf{R}^T\mathbf{J}^{-1} + \mathbf{M}_s \qquad (10)\\ \mathbf{M}_q &= \mathbf{J}^{-T}{}^B_P\mathbf{R}\,{}^P\mathbf{M}_x\,{}^B_P\mathbf{R}^T\mathbf{J}^{-1} - \\ &\quad \mathbf{J}^{-T}{}^B_P\mathbf{R}\,{}^P\mathbf{M}_x\,{}^U_P\mathbf{R}^T\mathbf{J}_c\mathbf{J}_B{}^{-1}. \qquad (11)\end{aligned}$$

$\mathbf{M}_p$ and $\mathbf{M}_q$ are joint space mass-inertia matrices.

3 Decoupling the Dynamics of Flexure Jointed Hexapods

McInroy et. al. [8] proposed two decoupling algorithms, which can be used in the "quiet box" problem (using payload acceleration, velocity, or position measurements to control the payload motion) and the "dirty box" problem (using base forces feedback to minimize the transmission of forces to the base). Their algorithms impose the following constraints:

1. The strut mass, damping, and stiffness matrices are scaled identities, $\mathbf{M}_s = m\mathbf{I}$, $\mathbf{B} = b\mathbf{I}$, $\mathbf{K} = k\mathbf{I}$.
2. The payload mass-inertia matrix (${}^B\mathbf{M}_x$) found with respect to frame $\{B\}$ is diagonal.
3. $\mathbf{J}^T\mathbf{J}$ is diagonal over the whole workspace.

In practice, the struts of a hexapod are usually identical. This means that the first constraint can be easily satisfied. Making ${}^B\mathbf{M}_x$ and $\mathbf{J}^T\mathbf{J}$ diagonal, in contrast, isn't an easy task.

The new algorithm still requires that constraint 1 be satisfied, but removes the much more restrictive constraints 2 and 3. The algorithm is suitable for both the "quiet box" and "dirty box" problems.

The payload mass-inertia matrix (${}^B\mathbf{M}_x$) is defined as [7]

$${}^B\mathbf{M}_x = {}^B_P\mathbf{R}\,{}^P\mathbf{M}_x\,{}^B_P\mathbf{R}^T = \begin{bmatrix} m_p\mathbf{I}_3 & \mathbf{0}_{3\times3} \\ \mathbf{0}_{3\times3} & {}^B_P\mathbf{R}\,{}^c\mathbf{I}\,{}^B_P\mathbf{R}^T \end{bmatrix} \qquad (12)$$

where m_p is the payload mass, ${}^c\mathbf{I}$ is the inertia tensor [3] of the payload with respect to the payload frame $\{P\}$, $\mathbf{I}_{3\times3}$ is a 3×3 identity matrix, and $\mathbf{0}_{3\times3}$ is a 3×3 zero matrix. It is obvious that ${}^B\mathbf{M}_x$ is symmetric.

Hence equation (10) implies that the joint space mass-inertia matrix $\mathbf{M}_p$ is symmetric. Since it is symmetric, $\mathbf{M}_p$ can be unitarily diagonalized [2]

$$\mathbf{M}_p = \mathbf{V}\mathbf{D}\mathbf{V}^T \qquad (13)$$

where $\mathbf{V}$ is an orthogonal matrix ($\mathbf{V}\mathbf{V}^T = \mathbf{V}^T\mathbf{V} = \mathbf{I}$), and $\mathbf{D}$ is a diagonal matrix.

For the "quiet box" problem, the dynamic model is described by the LTI equation (9). Laplace transforms can be taken to yield

$$\begin{aligned}(\mathbf{M}_p s^2 + \mathbf{B}s + \mathbf{K})\vec{p}_s = \vec{f}_m + \\ (\mathbf{M}_q s^2 + \mathbf{B}s + \mathbf{K})\vec{q}_s + \mathbf{J}^{-T}{}^U_B\mathbf{R}^T\vec{\mathcal{F}}_e \ . \qquad (14)\end{aligned}$$

Define a new input and a new output

$$\vec{u} = \mathbf{V}^T\vec{f}_m,\ \vec{y} = \mathbf{V}^T\vec{p}_s \ . \qquad (15)$$

Then (14) can be written as

$$(\mathbf{D}s^2+\mathbf{B}s+\mathbf{K})\vec{y}=\vec{u}+ \\ \mathbf{V}^T(\mathbf{M}_q s^2+\mathbf{B}s+\mathbf{K})\vec{q}_s+\mathbf{V}^T\mathbf{J}^{-T}{}_B^U\mathbf{R}^T\vec{\mathcal{F}}_e \ . \quad (16)$$

Note that the transfer matrix from $\vec{u}$ to $\vec{y}$ is diagonal. Consequently, the mapping from $\vec{u}$ to $\vec{y}$ is decoupled, and independent SISO controls can be designed. In addition to simplifying nominal control design, this also facilitates fault tolerant controls [10]. Based on (16), SISO LTI control algorithms can be designed to suppress the $\vec{q}_s$ and $\vec{\mathcal{F}}_e$ influences on the payload.

For "dirty box" vibration isolation applications, base forces are typically fed back, rather than payload positions, velocities or accelerations. The algorithm may be re-formulated to cover "dirty box" problems as follows. First, substituting (6) into (9), assuming $\vec{l_r}$ and $\vec{\mathcal{G}}$ terms cancel each other, solving for $\vec{f}_b$, and taking Laplace transforms gives

$$\vec{f}_b=\mathbf{M}_p s^2\vec{p}_s-\mathbf{M}_q s^2\vec{q}_s-\mathbf{J}^{-T}{}_B^U\mathbf{R}^T\vec{\mathcal{F}}_e \ . \quad (17)$$

Then by combining (14) and (17), we have

$$\vec{f}_b=\mathbf{M}_p s^2(\mathbf{M}_p s^2+\mathbf{B}s+\mathbf{K})^{-1}\vec{f}_m-\mathbf{M}_q s^2\vec{q}_s+ \\ \mathbf{M}_p s^2(\mathbf{M}_p s^2+\mathbf{B}s+\mathbf{K})^{-1}(\mathbf{M}_q s^2+\mathbf{B}s+\mathbf{K})\vec{q}_s+ \\ [\mathbf{M}_p s^2(\mathbf{M}_p s^2+\mathbf{B}s+\mathbf{K})^{-1}-\mathbf{I}]\mathbf{J}^{-T}{}_B^U\mathbf{R}^T\vec{\mathcal{F}}_e \ . \quad (18)$$

Define a new input and a new output

$$\vec{u}=\mathbf{V}^T\vec{f}_m,\ \vec{y}=\mathbf{V}^T\vec{f}_b \ . \quad (19)$$

Then (18) becomes

$$\vec{y}=\mathbf{D}s^2(\mathbf{D}s^2+\mathbf{B}s+\mathbf{K})^{-1}\vec{u}-\mathbf{V}^T\mathbf{M}_q s^2\vec{q}_s+ \\ \mathbf{D}s^2(\mathbf{D}s^2+\mathbf{B}s+\mathbf{K})^{-1}\mathbf{V}^T(\mathbf{M}_q s^2+\mathbf{B}s+\mathbf{K})\vec{q}_s+ \\ [\mathbf{D}s^2(\mathbf{D}s^2+\mathbf{B}s+\mathbf{K})^{-1}-\mathbf{I}]\mathbf{V}^T\mathbf{J}^{-T}{}_B^U\mathbf{R}^T\vec{\mathcal{F}}_e \ . \quad (20)$$

Once again, the dynamics from $\vec{u}$ to $\vec{y}$ is decoupled. SISO LTI compensators from $\vec{u}$ to $\vec{y}$ can be designed to suppress the base acceleration and exogenous force disturbances. Note that this can be viewed in two ways. If $\vec{\mathcal{F}}_e$ is the dominant disturbance, then the control provides dirty box isolation. If $\vec{q}_s$ is the dominant disturbance, then the hexapod attempts to quiet a vibrating structure.

4 Identification of Joint Space Mass-inertia Matrix

Section 3 shows that the dynamic model of a flexure jointed hexapod can be decoupled by transformations (15) or (19), in which $\mathbf{V}$ is an orthogonal matrix that diagonalizes the joint space mass-inertia matrix $\mathbf{M}_p$. In order to calculate $\mathbf{V}$, $\mathbf{M}_p$ must be known. There are two ways of obtaining $\mathbf{M}_p$. One way is to calculate $\mathbf{M}_p$ from the design parameters of the hexapod. The other is to identify $\mathbf{M}_p$ from measurements. The former method requires exact values of $\mathbf{M}_s$, ${}^P\mathbf{M}_x$, ${}_P^B\mathbf{R}$, and $\mathbf{J}$, which in practice is laborious to calculate and can introduce errors. This section derives a method of directly identifying $\mathbf{M}_p$ so performance can be retained despite manufacturing variances, payload changes, etc.

If the base is kept stationary and there are no exogenous generalized forces exerted on the payload when doing the identification experiment (these constraints can be easily satisfied) then $\ddot{\vec{q}}_s=\vec{0}$ and $\vec{\mathcal{F}}_e=\vec{0}$. Thus (17) becomes

$$\vec{f}_b=\mathbf{M}_p\ddot{\vec{p}}_s \ . \quad (21)$$

The accelerometer can only measure the acceleration along the strut direction, $\ddot{\vec{p}}_u$. The difference between $\ddot{\vec{p}}_s$ and $\ddot{\vec{p}}_u$ is that

$$\ddot{\vec{p}}_s=\ddot{\vec{p}}_u+\vec{\mathcal{C}}_1 \quad (22)$$

where $\vec{\mathcal{C}}_1$ is a vector of Coriolis terms. Compared with the magnitude of $\ddot{\vec{p}}_u$, $\vec{\mathcal{C}}_1$ is negligible. Thus (21) can be approximately written as

$$\vec{f}_b=\mathbf{M}_p\ddot{\vec{p}}_u \ . \quad (23)$$

This implies that if both the base forces ($\vec{f}_b$) and strut accelerations ($\ddot{\vec{p}}_u$) are measured, then $\mathbf{M}_p$ can be estimated. The main subtlety is that $\mathbf{M}_p$ is symmetric.

Now the identification problem is to find a matrix solution $\hat{\mathbf{M}}_p$ for equations

$$\hat{\vec{f}}_b^{\,k}=\hat{\mathbf{M}}_p\hat{\ddot{\vec{p}}}_u^{\,k},\ k=1,...,N \quad (24)$$

with the constraint $\hat{\mathbf{M}}_p$ being symmetric. N is the number of the samples, $\hat{\vec{f}}_b^{\,k}$ is the measured vector of base forces at time k, and $\hat{\ddot{\vec{p}}}_u^{\,k}$ is the measured vector of payload accelerations at time k.

By combining the N equations together, (24) can be written as

$$\mathbf{F}=\hat{\mathbf{M}}_p\mathbf{P} \quad (25)$$

where $\mathbf{F}=\left[\hat{\vec{f}}_b^{\,1},\ \hat{\vec{f}}_b^{\,2},\ ...,\ \hat{\vec{f}}_b^{\,N}\right]$, $\mathbf{P}=\left[\hat{\ddot{\vec{p}}}_u^{\,1},\ \hat{\ddot{\vec{p}}}_u^{\,2},\ ...,\ \hat{\ddot{\vec{p}}}_u^{\,N}\right]$.

Higham [6] shows that if $\mathbf{P}$ is full rank, then the unique constrained LS solution of (25) is given by the solution of the Lyapunov equation

$$\mathbf{P}\mathbf{P}^T\hat{\mathbf{M}}_p+\hat{\mathbf{M}}_p\mathbf{P}\mathbf{P}^T=\mathbf{P}\mathbf{F}^T+\mathbf{F}\mathbf{P}^T. \quad (26)$$

Note that the data in $\mathbf{P}$ is the acceleration and as a result $\mathbf{P}$ is corrupted with noise. Thus the estimation given by (26) is biased. Many other approaches, such as the Total Least Squares and Maximum Likelihood, etc., can overcome this problem.

5 Experimental Results

The identification and decoupling algorithms have been experimentally verified on one of the UW's mutually orthogonal hexapods. The mechanical parts of the hexapod are all custom machined based on a NASA Jet Propulsion Laboratory design. A 200 MHz Gateway 2000 Pentium II computer running the QNX real time operating system sends commands through Computers Boards 16 bit DAC converters to Techron linear current amplifiers. These power BEI voice coil actuators, resulting in base forces ($\vec{f}_b$) measured by PCB quartz force rings mounted on the bottom end of each strut, and payload accelerations ($\ddot{\vec{p}}_u$) measured by KISTLER-BEAM accelerometers mounted on the top of the spherical joint connecting the payload. The force and acceleration signals are sampled by the control computer's 16 bit A/D converters at a rate of 5kHz. Each strut has a maximum stroke of $\pm$ .025 inches.

For the identification experiment, six independent random-noise signals pass through six digital low-pass filters with cutoff frequencies at 80Hz. Then the filtered signals are sent to all six voice coil actuators to generate vibrations. 256K samples (each sample includes 6 base forces and 6 payload accelerations) are collected. Based on (26), $\hat{\mathbf{M}}_p$ is calculated.

The performance of the new algorithm will be compared to that obtained using the algorithm in [8]. In [8], a new input and a new output are defined as

$$\vec{u} = \mathbf{J}^T \vec{f}_m,\ \vec{y} = \mathbf{J}^T \vec{f}_b \ . \tag{27}$$

Bode magnitude plots from u_5 (input of channel 5) to $\vec{y}$ (all six channels) are shown in Figure 2.

Using the $\mathbf{M}_p$ matrix calculated from the design parameters of the hexapod, a new input and a new output are defined using (19). Bode magnitude plots from u_5 to $\vec{y}$ are shown in Figure 3.

Finally using the results of the identification experiment ($\hat{\mathbf{M}}_p$) a new input and a new output are found from (19). Bode magnitude plots from u_5 to $\vec{y}$ are shown in Figure 4.

In the experiment, the payload's center of mass doesn't coincide with the center of the cube formed

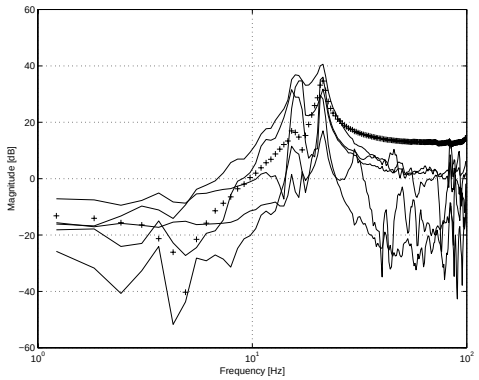

Figure 2: Using $\mathbf{J}^T$ as decoupling matrix. Bode magnitude plots from u_5 to $\vec{y}$. y_5 is denoted by "+" signs.

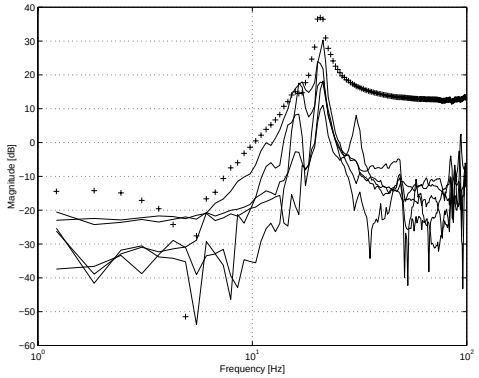

Figure 3: Using $\mathbf{V}^T$ as decoupling matrix ($\mathbf{V}^T$ is calculated from $\mathbf{M}_p$). Bode magnitude plots from u_5 to $\vec{y}$. y_5 is denoted by "+" signs.

by the orthogonal struts. From Figure 2, we can see that using decoupling transform (27), there are still strong couplings among all six channels. The input channel (channel 5) is difficult to distinguish from the others. Using the calculated $\mathbf{M_p}$ matrix and the new decoupling transform (19), channel 5 is 3 times (10 dB) stronger (Figure 3). When the estimated joint space mass-inertia matrix $\hat{\mathbf{M}}_p$ and the new decoupling transform (19) are used, channel 5 is almost 10 times (20dB) stronger across nearly all frequencies (in Figure 4).

6 Conclusions

A new decoupling algorithm is derived using the symmetric property of the joint space mass-inertia matrix

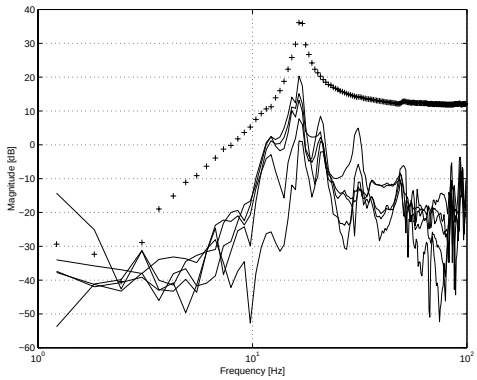

Figure 4: Using $\mathbf{V}^T$ as decoupling matrix ($\mathbf{V}^T$ is calculated from $\hat{\mathbf{M}}_p$). Bode magnitude plots from u_5 to $\vec{y}$. y_5 is denoted by "+" signs.

($\mathbf{M}_p$). Compared to the earlier decoupling methods [8], the new algorithm puts far less constraints on the geometric and payload design of a hexapod because it does not require ${}^B\mathbf{M}_x$ and $\mathbf{J}^T\mathbf{J}$ to be diagonal. Thus greatly expands the potential applications. In order to get the new decoupling matrix, $\mathbf{V}$, $\mathbf{M}_p$ must be known. While $\mathbf{M}_p$ can be calculated by system parameters, the process is cumbersome when the payload changes often, and is sensitive to modeling errors. Consequently, a method for identification of $\mathbf{M}_p$ is derived. Experimental results verify that the new approaches are practical, and yield good performance.

Acknowledgments

This work was supported by the Ballistic Missile Defense Organization and Army Research Office under grant DAAG55-98-1-0007.

References

[1] E. H. Anderson, D. J. Leo, and M. D. Holcomb, "Ultraquiet platform for active vibration isolation," in *Proceedings of the SPIE Smart Structure and Materials Conference,* pp. 436-451, 1996.

[2] C. T. Chen, *Linear System Theory and Design,* Holt Rinehart, NY: CBS College Publishing, 1984.

[3] J. J. Craig, *Itroduction to Robotics: Mechanics and Control,* Reading, MA: Addison-Wesley, 1986.

[4] Z. J. Geng and L. S. Haynes, "Six degree-of-freedom active vibration control using the Stewart platforms," *IEEE Transactions on Control Systems Technology,* vol. 2, pp. 45-53, March 1994.

[5] Z. J. Geng, G. G. Pan, L. S. Haynes, B. K. Wada, and J. A. Garba, "An intelligent control system for multiple degree-of-freedom vibration isolation," *Journal of Intelligent Material Systems and Structures,* vol. 6, pp. 787-800, November 1995.

[6] N. J. Higham, "The Symmetric Procrustes Problem," *BIT,* 28, pp. 133-143, 1988.

[7] J. E. McInroy, "Dynamic Modeling of Flexure Jointed Hexapods for Control Purposes," *IEEE Conference on Control Applications,* (Kona, Hawaii), pp. 508-513, August 1999.

[8] J. E. McInroy and J. C. Hamann, "Design and Control of Flexure Jointed Hexapods," *IEEE Transactions on Robotics and Automation,* Accepted and awaiting publiction.

[9] J. E. McInroy, J. F. O'Brien, and G. Neat, "Method and experimental validation of a precision, reconfigurable pointing control strategy," in *IEEE Conference on Decision and Control,* (San Diego, CA), December 1997.

[10] J. E. McInroy, J. F. O'Brien, and G. W. Neat, "Precise, fault tolerant pointing using a Stewart platform," *IEEE/ASME Transactions on Mechatronics,* vol. 4, pp. 91-95, March 1999.

[11] J. F. O'Brien, J. E. McInroy, D. Bodtke, M. Bruch, and J. C. Hamann, "Lessons learned in nonlinear systems and flexible robots through experiments on a 6 legged platform," in *American Control Conference,* (Philadelphia, PA), pp. 868-872, 1998.

[12] J. Spanos, Z. Rahman, and G. Blackwood, "A soft 6-axis active vibration isolator," in *Proceedings of the American Control Conference,* pp. 412-416, 1995.

[13] J. Sullivan, A. Rahman, R. Cobb, and J. Spanos, "Closed-loop performance of a vibration isolation and suppression system," in *Proceedings of the American Control Conference,* pp. 3974-3978, 1997.

[14] D. Thayer, J. Vagners, A. von Flotow, C. Hardham, and K. Scribner, "Six-axis vibration isolation systems using soft actuators and multiple sensors," in *Proceedings of the Annual American Astronautical Society (AAS) Rocky Mountain Guidance and Control Conference,* pp. 497-506, 1998.